Dual Spin Excitation Components in $FeSe_{0.67}Te_{0.33}$

Hao Zhang,[1] Hongliang Wo,[1] Yimeng Gu,[1] Zeyu Kao,[1] Gaofeng Ding,[1] Kazuki Iida,[2] Kazuhiko Ikeuchi,[3,4] and Jun Zhao[1,5,6,*]

[1]State Key Laboratory of Surface Physics and Department of Physics, Fudan University, Shanghai 200433, China
[2]Neutron Science and Technology Center, Comprehensive Research Organization for Science and Society (CROSS), Tokai 319-1106, Ibaraki, Japan
[3]Materials and Life Science Division, J-PARC Center, Tokai, Ibaraki 319-1195, Japan
[4]Institute of Materials Structure Science, High Energy Accelerator Research Organization (KEK), Tokai, Ibaraki 319-1106, Japan
[5]Shanghai Research Center for Quantum Sciences, Shanghai 201315, China
[6]Institute of Nanoelectronics and Quantum Computing, Fudan University, Shanghai 200433, China

(Received 3 July 2025; revised 22 November 2025; accepted 24 February 2026; published 11 March 2026)

Iron chalcogenide superconductors $FeSe_{1-x}Ch_x$ (Ch = S, Te) exhibit an unusual double-dome superconducting phase diagram, the microscopic origin of which remains unclear. Here, we use inelastic neutron scattering to probe spin excitations in single-crystalline $FeSe_{0.67}Te_{0.33}$, positioned at the superconducting transition temperature (T_c) minimum between the two domes. We identify two distinct spin excitation components separated by a crossover energy ($E_c \approx 30$ meV). Below E_c the spin excitations emanate from the stripe-type wave vector (1,0), with their intensity strongly suppressed upon warming above the nematic transition at $T_s \approx 40$ K, revealing strong coupling between them. Above E_c the high-energy excitations disperse more steeply and display little temperature dependence across T_s. Further warming from T_s to 300 K results in the gradual downward evolution of the high-energy spin excitations, reaching an incommensurate wave vector near $(1, \pm 0.3)$ at the low-energy limit. The combined energy- and temperature-dependent responses point to competition between stripe and incommensurate excitations, which can contribute to the reduced T_c near the valley composition; while Te substitution may simultaneously tune the electronic structure in ways that could coexist with, or reinforce, this competition. These findings illuminate the intricate interplay of multiple components of magnetic excitations in shaping T_c of iron chalcogenides.

DOI: 10.1103/fbfp-7gw6

Understanding the intertwined roles of magnetism, nematicity, and superconductivity in iron-based superconductors is essential for identifying the pairing mechanism of high-temperature superconductivity [1–6]. Owing to its simple crystallographic structure, intriguing magnetic and nematic properties, and highly tunable superconductivity, FeSe has become a prototype material for such studies [7–9]. It undergoes a tetragonal-to-orthorhombic nematic transition at $T_s \approx 90$ K without developing long-range stripe-type antiferromagnetic order down to 2 K [2]. Inelastic neutron-scattering experiments revealed coexisting stripe- and Néel-type spin fluctuations over a broad energy window in the paramagnetic state; these fluctuations are strongly coupled to nematic order [10–12].

FeSe is also intriguing because both positive and negative chemical pressure, achieved respectively by S and Te substitution, allow continuous tuning of nematicity, magnetism, and superconductivity, thereby providing an ideal platform to disentangle their mutual couplings [13–17]. Replacing Se with the heavier Te enhances the spin-orbit interaction relative to FeSe and $FeSe_{1-x}S_x$, an effect believed to be important for the intertwined superconducting, nematic, magnetic, and topological phenomena in the iron chalcogenides [18–20].

Previous studied compositions mainly lie on the Te-rich side ($x > 0.5$) [21–28]. Breakthroughs in crystal growth have only recently yielded phase-pure single crystals on the Se-rich side ($x < 0.5$), enabling a detailed phase diagram close to the FeSe end member [13,29]. With increasing Te content, the nematic transition temperature decreases monotonically, extrapolating to zero near $x \approx 0.5$, indicative of a possible nematic quantum critical point. In contrast, the superconducting transition temperature T_c exhibits a nonmonotonic evolution: it drops to a local minimum of approximately 6 K at $x \approx 0.3$ before rising again to 14.5 K at $x \approx 0.56$ [13,14,23,29]. When combined with the S-doped phase diagram, these data reveal a striking double-dome structure separated by the low-T_c valley at $x \approx 0.3$ [Fig. 1(a)] [14]. The microscopic origin of this two-dome behavior, particularly the local minimum in T_c at $x \approx 0.3$, remains elusive, suggesting the involvement of an

*Contact author: zhaoj@fudan.edu.cn

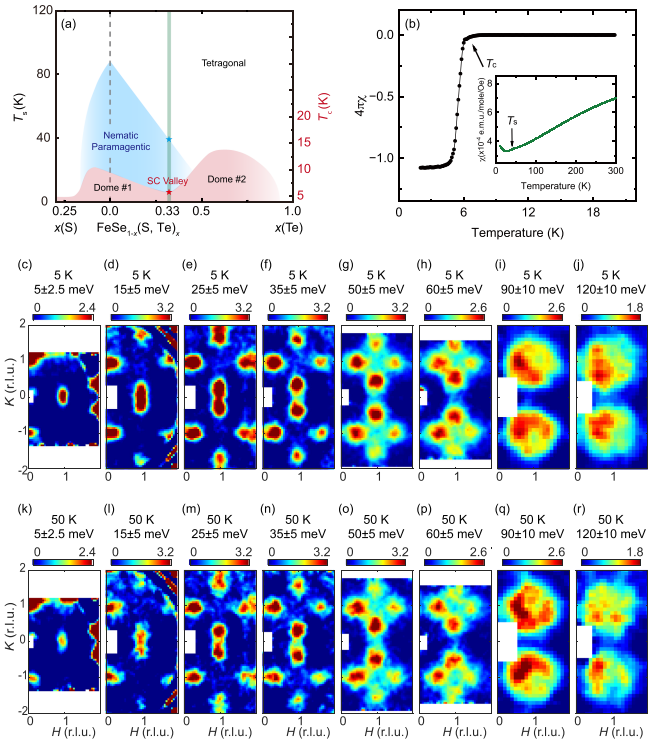

FIG. 1. (a) Temperature-doping phase diagram of $FeSe_{1-x}(S,Te)_x$. The nematic and superconducting transition temperatures of our 33% Te doping sample are marked as stars. The doping range of our samples are indicated by the vertical green bar in the phase diagram. (b) dc magnetic susceptibility of our $FeSe_{0.67}Te_{0.33}$ single crystals. Zero-field-cooled (ZFC) magnetic susceptibility measured in a magnetic field of $H = 10$ Oe. A sharp superconducting transition is observed at ≈6 K. Magnetic susceptibility under a magnetic field of $H = 70000$ Oe. The kink at 40 K corresponds to the structural (nematic) phase transition. Constant-energy schematic images of spin fluctuations in $FeSe_{0.67}Te_{0.33}$ projected onto the (H, K) plane at 5 and 50 K. (c)–(j) Constant-energy plots at 5 K at energy transfers $E = 5 \pm 2.5$ $(E_i = 27.20)$, $E = 15 \pm 5$, 25 ± 5, 35 ± 5, 50 ± 5, 60 ± 5 $(E_i = 95.36)$, and $E = 90 \pm 10$, 120 ± 10 meV $(E_i = 300.00$ meV). (k)–(r) Constant-energy plots obtained at 50 K at the same energy transfers and same intensity scale as those acquired at 5 K. All of the measurements were carried out on 4SEASONS with the c axis parallel to the incident beam. The sample has two equally populated orthogonal twin domains in the ab plane at 5 K and the intensities near (1,0) and (0,1) are roughly the same. Symmetry equivalent data were pooled to enhance statistical accuracy. The data have been subtracted by a radical isotropic background. The color bars indicate intensity in unit of mbar sr^{-1} meV^{-1} f.u.$^{-1}$.

additional electronic degree of freedom. This makes a detailed investigation of spin excitations in $FeSe_{1-x}Te_x$ crystals at the T_c valley of $x \approx 0.3$ especially compelling.

In this Letter, we used inelastic neutron scattering to study spin-fluctuation spectra over the entire Brillouin zone in single-crystalline $FeSe_{0.67}Te_{0.33}$ (Supplemental Material [30], see also Refs. [10,29,31–33] therein). High-quality $FeSe_{0.67}Te_{0.33}$ single crystals were grown by the chemical vapor transport method using eutectic $AlCl_3/KCl$ as the transport agent. The specific heat, magnetic susceptibility, and resistivity measurements performed on randomly selected $FeSe_{0.67}Te_{0.33}$ single crystals consistently suggest the nematic ordering temperature of $T_s \approx 40$ K and superconducting transition temperature of $T_c \approx 6$ K [Figs. 1(a) and 1(b)]. Our inelastic neutron-scattering measurements were carried out on the 4SEASONS chopper spectrometer at the Japan Proton Accelerator Research Complex. The large detector arrays on this instrument allowed us to measure spin excitations over a wide range of energy and momentum. The $|\mathbf{Q}|$-dependent background is subtracted for the data below the aluminum phonon cutoff energy of 40 meV (Supplemental Material [30], see also Refs. [10,29,31–33] therein). To facilitate comparison with theory and previous measurements, our data were normalized into absolute units by using the elastic incoherent scattering of a standard vanadium sample. The incident neutron beam was aligned parallel to the c axis because of the anticipated two-dimensional nature of the magnetism [10,21]. Under this setup, the energy transfer was coupled with L. We define the wave vector $\mathbf{Q}$ in three-dimensional reciprocal space (in units of Å^{-1}) as $\mathbf{Q} = H\mathbf{a}^* + K\mathbf{b}^* + L\mathbf{c}^*$, where H, K, and L are Miller indices and $\mathbf{a}^* = (2\pi/a)\hat{\mathbf{a}}$, $\mathbf{b}^* = (2\pi/b)\hat{\mathbf{b}}$, $\mathbf{c}^* = (2\pi/c)\hat{\mathbf{c}}$ are reciprocal lattice units of the orthorhombic unit cell, where $a \approx 5.35$, $b \approx 5.35$, and $c \approx 5.8$ Å. In this unit cell, the magnetic wave vector associated with the stripe order is $\mathbf{Q} = (1, 0)$.

Figure 1 presents the measured spin fluctuations at several energy transfers in the (H, K) plane both above and below T_s. In the low-temperature nematic phase (5 K), the spin response is strongest at $\mathbf{Q} = (1, 0)$ at 5 meV [Fig. 1(c)]. With an increase in energy, the spin fluctuations show anisotropic dispersion and elongate along the K direction, which is analogous to the stripe spin fluctuations detected in FeSe and other iron-based superconductors [10,21]. No discernible scattering is observed arising from (1,1), indicating that Te substitution steers the system away from the competing Néel instability. At energies up to ≈25 meV, the elliptical scattering elongating along the K direction split to two branches, and with further energy increase, these scatterings overlap, eventually merging into a broad region centered at (1,1) above 120 meV. Upon warming to the tetragonal phase (50 K), scattering associated with stripe fluctuations below $E_c \approx 30$ meV weakens significantly.

To further elucidate the spin excitation dispersion in $E - \mathbf{Q}$ space, we projected the stripe spin fluctuations along the K direction near (1,0) (Fig. 2). It is shown that the spin fluctuations exhibit a rather unusual dispersion in the nematic phase. At low energies, the fluctuations arise from the commensurate (1,0) position and split into two branches as energy increases, displaying nearly linear dispersion up to 30 meV. Above 30 meV, the dispersion increases in velocity, with a kink feature appearing around 30 meV. The differing dispersions suggest that the low-energy and high-energy spin

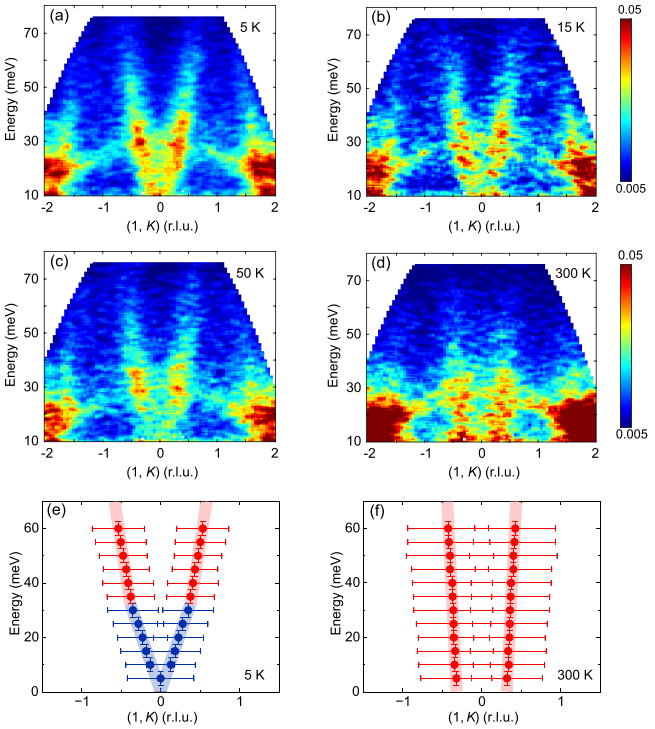

FIG. 2. Dispersions of the observed spin fluctuations at $5-300$ K. (a)–(d) Dispersions of the observed spin fluctuations at 5, 15, 50, and 300 K, respectively. The data were collected on 4SEASONS by using incident energy of 95.36 meV. Obvious suppression of low-energy signals above T_s is shown. (e), (f) Extracted dispersion acquired from constant-energy cuts near (1,0) along the K direction at 5 and 300 K, respectively. The points represent the peak positions fitted with Gaussians. The errors in energy are the energy integration range and the $\mathbf{Q}$ errors come from the fitted peak width. The color bars indicate intensity in arbitrary unit of raw data.

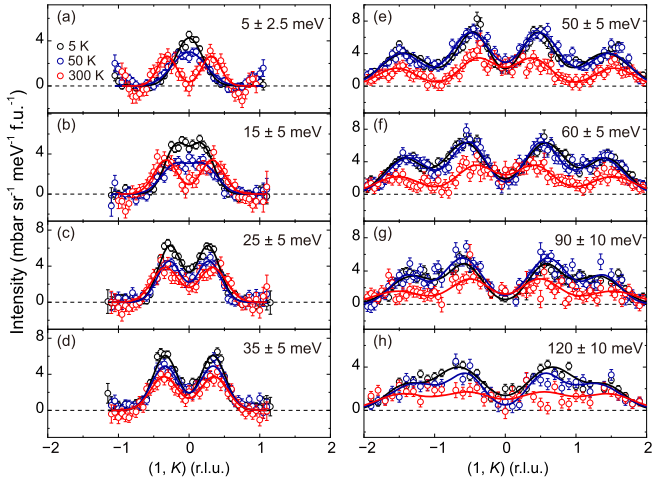

FIG. 3. (a)–(h) Constant-energy cuts through the stripe magnetic wave vector along the transverse direction at 5, 50, and 300 K. The peak positions are determined by fitting with Gaussian profiles convoluted with the instrumental resolution, with the Fe^{2+} magnetic form factor corrected. The error bars indicate 1 s.d.

excitations arise from different mechanisms. On warming to 50 K above T_s, the high-energy spin excitations show little change, while the strength of the low-energy fluctuations significantly decreases. These contrasting behaviors of high- and low-energy spin fluctuations further suggest distinct origins for each [34–36].

To further understand the nature of high-energy and low-energy spin excitations in this system, we performed measurements on a wider temperature range from 5 to 300 K. The evolution of dispersions with temperature is shown in Figs. 2(a)–2(d). As is clearly seen, the high-energy part remains basically unchanged across the entire temperature range, all showing steep upward dispersions. On warming, these excitations evolve downward and reach an incommensurate position of around $(1, \pm 0.3)$ in the low-energy limit at 300 K, but no static magnetic order is observed, suggesting the presence of dynamic and short-range magnetic correlations (Supplemental Material Fig. S2 [30]). The incommensurate excitations near $(1, \pm 0.3)$ are distant from the ordering vector (0.5,0.5) of FeTe [27,28] and, therefore, are unlikely to be related to the double-stripe magnetic instability. The shift in spectral weight from the stripe to the incommensurate positions indicates a competition between the two.

To quantify the dispersions and intensities of the spin fluctuations, we made constant-energy cuts at various energies and temperatures (Fig. 3). These measurements quantitatively confirm the temperature evolution of the spin fluctuations discussed earlier. The detailed temperature dependence of stripe spin fluctuations at 17 meV displayed an order parameterlike behavior across T_s, suggesting the low-energy spin fluctuations are coupled with nematicity [Fig. 4(a)]. In contrast, the higher-energy component shows only a weak temperature dependence and no discernible anomaly at T_s [Fig. 4(b)].

We also calculated the energy dependence of the momentum integrated local dynamical susceptibility $\chi''(\omega)$ in absolute units to gain a more comprehensive understanding of the evolution of magnetism with Te doping. The local susceptibility was obtained by averaging the spin spectral weight over the Brillouin zone, followed by the Bose factor correction. As Fig. 4(c) shows, the momentum integrated local dynamical susceptibility exhibits a broad peak at around 60 meV and extends to 200 meV. Comparing to its parent compound FeSe, the bandwidth of magnetic excitations narrows and the spectral weight transfers to lower energy globally [10,11].

To obtain the overall strength of the magnetic excitations, the local fluctuating moment $\langle m^2 \rangle$ can be computed by integrating $\chi''(\omega)$ in the whole magnetic bandwidth up to band top at 200 meV. The calculated $\langle m^2 \rangle = (g\mu_B)^2 S(S+1) = (6.85 \pm 0.10)\mu_B^2/\mathrm{Fe}$, corresponding to an effective spin $S \approx 0.90$ in $FeSe_{0.67}Te_{0.33}$. This value is larger than that in FeSe [$\langle m^2 \rangle = (5.19 \pm 0.32)\mu_B^2/\mathrm{Fe}$ and $S \approx 0.74$].

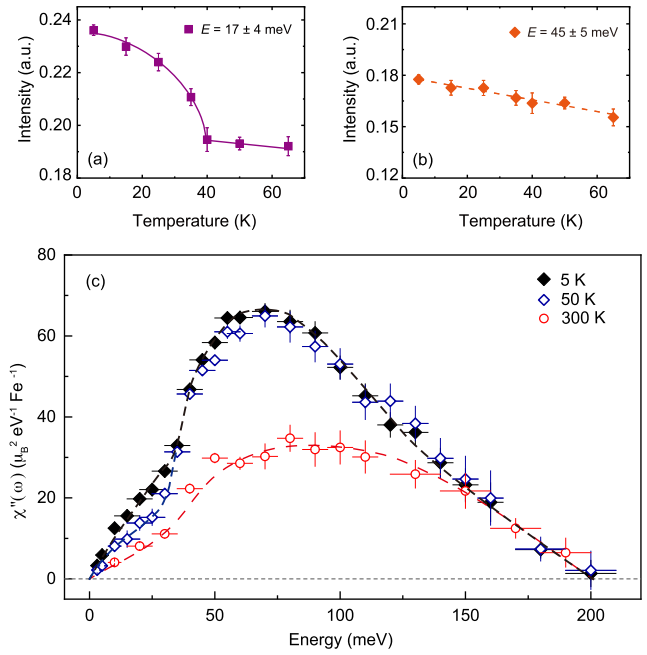

FIG. 4. (a),(b) Temperature dependence of the intensities of the stripe and incommensurate spin fluctuations across T_s. Detailed intensity change with temperature at two different energy levels are plotted. Low-energy spin excitations at 17 meV showed an order parameterlike behavior with nematic transition. However, high-energy spin excitations at 45 meV changed negligibly with increasing temperature. (c) Energy dependence of the local susceptibility $\chi''(\omega)$ at 5, 50, and 300 K. The data were collected on 4SEASONS with $E_i = 300.00, 95.36$, and 27.20 meV. The horizontal and vertical bars indicated the energy integration range, and the statistical errors of 1 s.d., respectively.

The dispersion and temperature evolution of spin excitations in $FeSe_{0.67}Te_{0.33}$ highlight the dual nature of magnetic fluctuations. At low energies, the stripe-type excitations couple strongly to nematic order, resembling behaviors observed in FeSe and iron pnictides, where stripe magnetic instabilities may drive nematic transitions [37–40]. Conversely, the high-energy excitations show little temperature dependence and are largely unaffected by nematicity, likely rooted in the d_{xy} orbital which is believed to be more strongly correlated and localized [36,41–44]. Tellurium substitution enhances this localized component, producing a dispersion that is qualitatively different from the low-energy stripe excitations below 30 meV.

Electronic structure measurements have revealed that in $FeSe_{1-x}Te_x$ with $x = 0.33$, the top of the hole band derived from the d_{xy} orbital lies approximately 20–30 meV below the Fermi level at the Γ point [39,43]. This energy offset aligns with the local component of spin excitations observed above 30 meV. Because these incommensurate excitations occur at distinct wave vectors that are not obviously connected by a simple Fermi-surface nesting condition, they may not efficiently promote superconducting pairing and instead compete with the stripe fluctuations, which may lead to a suppression of superconductivity [10,17]. With further increasing Te substitution, the flat d_{xy} hole band at Γ gradually moves upward and eventually touches the Fermi level, allowing the d_{xy} electrons to participate in Cooper pairing [39,43]. This evolution may enhance superconductivity and give rise to the second superconducting dome [Fig. 1(a)].

More broadly, Te substitution tunes not only the d_{xy} band position discussed above, but also the degree of orbital selectivity and electronic correlations, which can reshape the balance among spin-fluctuation channels. In this context, the competition between stripelike and incommensurate excitations identified here provides a microscopic magnetic ingredient that can accompany Te-driven electronic reconstruction across the phase diagram.

Moreover, the fact that momentum-integrated $\chi''(\omega)$ exhibits a narrower bandwidth signals the strengthened electronic correlations [45]. This is further confirmed by the larger local fluctuating moment, $\langle m^2 \rangle$ and effective spin $S \approx 0.90$ in $FeSe_{0.67}Te_{0.33}$, compared with that (0.74) in pure FeSe. This is consistent with the expectation that stronger electronic correlations induced by Te substitution drives the system closer to a localized $S = 1$ state [42,46,47].

Upon warming from 50 to 300 K (tetragonal phase), the dispersions convert to two rods-like feature near an incommensurate wave vector away from the stripe wave vector. Remarkably, such transformation is reminiscent of the evolution from a twisted hourglass to rodlike feature in hole-doped cuprates in the pseudogap state [48,49], suggesting a potentially shared microscopic mechanism. In $FeSe_{0.67}Te_{0.33}$, this behavior may originate from an orbital-selective Mott crossover that progressively localizes the Fe $3d_{xy}$ orbital states [42,50,51]. It will be particularly interesting to explore whether a similar Mottness-driven reconstruction underlies the pseudogap in cuprates.

In summary, we have carried out inelastic neutron scattering measurements on single-crystalline $FeSe_{0.67}Te_{0.33}$ across a broad range of energy, momentum, and temperature. Our results reveal distinct dispersion and temperature-dependent behaviors in the low- and high-energy spin excitations, reflecting a dual nature of magnetic fluctuations. The unusual phase diagram in $FeSe_{1-x}Ch_x$ may be viewed as a macroscopic manifestation of the interplay between spin fluctuations with different characters, and their competition may contribute to the local minimum in T_c. This magnetic competition can coexist with other Te-tuned electronic changes, together shaping the evolution of superconductivity. Our findings highlight the critical influence of multiple-component spin excitations on T_c and nematicity in iron chalcogenides, offering valuable microscopic insights into the underlying mechanisms driving unconventional superconductivity.

Acknowledgments—This work was supported by the Key Program of National Natural Science Foundation of China

(Grant No. 12234006), the National Key R&D Program of China (Grant No. 2022YFA1403202), the Quantum Science and Technology-National Science and Technology Major Project (Grant No. 2024ZD0300103), the Shanghai Municipal Science and Technology Project (Grants No. 25DZ3008100 and No. 2019SHZDZX01), and the Large Scientific Facility Open Subject of Songshan Lake Laboratory (Grant No. KFKT2022A03). The neutron experiments at 4SEASONS (BL-01) were carried out under approval of the Materials and Life Science Experimental Facility of the J-PARC (Proposal No. 2023A0045).

Data availability—The data that support the findings of this article are not publicly available upon publication because it is not technically feasible and/or the cost of preparing, depositing, and hosting the data would be prohibitive within the terms of this research project. The data are available from the authors upon reasonable request.

[1] P. Dai, Antiferromagnetic order and spin dynamics in iron-based superconductors, Rev. Mod. Phys. **87**, 855 (2015).

[2] T. M. McQueen, A. J. Williams, P. W. Stephens, J. Tao, Y. Zhu, V. Ksenofontov, F. Casper, C. Felser, and R. J. Cava, Tetragonal-to-orthorhombic structural phase transition at 90 K in the superconductor $Fe_{1.01}Se$, Phys. Rev. Lett. **103**, 057002 (2009).

[3] F. Wang, S. A. Kivelson, and D.-H. Lee, Nematicity and quantum paramagnetism in FeSe, Nat. Phys. **11**, 959 (2015).

[4] J. K. Glasbrenner, I. I. Mazin, H. O. Jeschke, P. J. Hirschfeld, R. M. Fernandes, and R. Valentí, Effect of magnetic frustration on nematicity and superconductivity in iron chalcogenides, Nat. Phys. **11**, 953 (2015).

[5] A. E. Böhmer and A. Kreisel, Nematicity, magnetism and superconductivity in FeSe, J. Phys. Condens. Matter **30**, 023001 (2018).

[6] H.-Y. Cao, S. Chen, H. Xiang, and X.-G. Gong, Antiferromagnetic ground state with pair-checkerboard order in FeSe, Phys. Rev. B **91**, 020504(R) (2015).

[7] A. V. Chubukov, R. M. Fernandes, and J. Schmalian, Origin of nematic order in FeSe, Phys. Rev. B **91**, 201105(R) (2015).

[8] R. Yu and Q. Si, Antiferroquadrupolar and ising-nematic orders of a frustrated bilinear-biquadratic Heisenberg model and implications for the magnetism of FeSe, Phys. Rev. Lett. **115**, 116401 (2015).

[9] J.-F. Ge, Z.-L. Liu, C. Liu, C.-L. Gao, D. Qian, Q.-K. Xue, Y. Liu, and J.-F. Jia, Superconductivity above 100 K in single-layer FeSe films on doped $SrTiO_3$, Nat. Mater. **14**, 285 (2015).

[10] Q. Wang, Y. Shen, B. Pan, X. Zhang, K. Ikeuchi, K. Iida, A. D. Christianson, H. C. Walker, D. T. Adroja, M. Abdel-Hafiez, X. Chen, D. A. Chareev, A. N. Vasiliev, and J. Zhao, Magnetic ground state of FeSe, Nat. Commun. **7**, 12182 (2016).

[11] R. Liu, M. B. Stone, S. Gao, M. Nakamura, K. Kamazawa, A. Krajewska, H. C. Walker, P. Cheng, R. Yu, Q. Si, P. Dai, and X. Lu, Nematic quantum disordered state in FeSe, arXiv:2401.05092.

[12] Q. Wang, Y. Shen, B. Pan, Y. Hao, M. Ma, F. Zhou, P. Steffens, K. Schmalzl, T. R. Forrest, M. Abdel-Hafiez, X. Chen, D. A. Chareev, A. N. Vasiliev, P. Bourges, Y. Sidis, H. Cao, and J. Zhao, Strong interplay between stripe spin fluctuations, nematicity and superconductivity in FeSe, Nat. Mater. **15**, 159 (2016).

[13] K. Mukasa, K. Matsuura, M. Qiu, M. Saito, Y. Sugimura, K. Ishida, M. Otani, Y. Onishi, Y. Mizukami, K. Hashimoto, J. Gouchi, R. Kumai, Y. Uwatoko, and T. Shibauchi, High-pressure phase diagrams of $FeSe_{1-x}Te_x$: Correlation between suppressed nematicity and enhanced superconductivity, Nat. Commun. **12**, 381 (2021).

[14] K. Ishida, Y. Onishi, M. Tsujii, K. Mukasa, M. Qiu, M. Saito, Y. Sugimura, K. Matsuura, Y. Mizukami, K. Hashimoto, and T. Shibauchi, Pure nematic quantum critical point accompanied by a superconducting dome, Proc. Natl. Acad. Sci. U.S.A. **119**, e2110501119 (2022).

[15] K. Matsuura *et al.*, Maximizing T_c by tuning nematicity and magnetism in $FeSe_{1-x}S_x$ superconductors, Nat. Commun. **8**, 1143 (2017).

[16] S. Hosoi, K. Matsuura, K. Ishida, H. Wang, Y. Mizukami, T. Watashige, S. Kasahara, Y. Matsuda, and T. Shibauchi, Nematic quantum critical point without magnetism in $FeSe_{1-x}S_x$ superconductors, Proc. Natl. Acad. Sci. U.S.A. **113**, 8139 (2016).

[17] W. Bao, Y. Qiu, Q. Huang, M. A. Green, P. Zajdel, M. R. Fitzsimmons, M. Zhernenkov, S. Chang, M. Fang, B. Qian, E. K. Vehstedt, J. Yang, H. M. Pham, L. Spinu, and Z. Q. Mao, Tunable $(\delta\pi, \delta\pi)$-type antiferromagnetic order in α-Fe(Te, Se) superconductors, Phys. Rev. Lett. **102**, 247001 (2009).

[18] M. Ma, P. Bourges, Y. Sidis, Y. Xu, S. Li, B. Hu, J. Li, F. Wang, and Y. Li, Prominent role of spin-orbit coupling in FeSe revealed by inelastic neutron scattering, Phys. Rev. X **7**, 021025 (2017).

[19] J. Li, B. Lei, D. Zhao, L. P. Nie, D. W. Song, L. X. Zheng, S. J. Li, B. L. Kang, X. G. Luo, T. Wu, and X. H. Chen, Spin-orbital-intertwined nematic state in FeSe, Phys. Rev. X **10**, 011034 (2020).

[20] Y.-F. Li, S.-D. Chen, M. García-Díez, M. I. Iraola, H. Pfau, Y.-L. Zhu, Z.-Q. Mao, T. Chen, M. Yi, P.-C. Dai, J. A. Sobota, M. Hashimoto, M. G. Vergniory, D.-H. Lu, and Z.-X. Shen, Orbital ingredients and persistent dirac surface state for the topological band structure in $FeTe_{0.55}Se_{0.45}$, Phys. Rev. X **14**, 021043 (2024).

[21] M. D. Lumsden, A. D. Christianson, E. A. Goremychkin, S. E. Nagler, H. A. Mook, M. B. Stone, D. L. Abernathy, T. Guidi, G. J. MacDougall, C. De La Cruz, A. S. Sefat, M. A. McGuire, B. C. Sales, and D. Mandrus, Evolution of spin excitations into the superconducting state in $FeTe_{1-x}Se_x$, Nat. Phys. **6**, 182 (2010).

[22] T. J. Liu *et al.*, From $(\pi, 0)$ magnetic order to superconductivity with (π, π) magnetic resonance in $Fe_{1.02}Te_{1-x}Se_x$, Nat. Mater. **9**, 718 (2010).

[23] B. C. Sales, A. S. Sefat, M. A. McGuire, R. Y. Jin, D. Mandrus, and Y. Mozharivskyj, Bulk superconductivity at 14 K in single crystals of $Fe_{1+y}Te_xSe_{1-x}$, Phys. Rev. B **79**, 094521 (2009).

[24] R. Khasanov, M. Bendele, A. Amato, P. Babkevich, A. T. Boothroyd, A. Cervellino, K. Conder, S. N. Gvasaliya,

H. Keller, H.-H. Klauss, H. Luetkens, V. Pomjakushin, E. Pomjakushina, and B. Roessli, Coexistence of incommensurate magnetism and superconductivity in $Fe_{1+y}Se_xTe_{1-x}$, Phys. Rev. B **80**, 140511(R) (2009).

[25] Y. Liu, R. K. Kremer, and C. T. Lin, Doping evolution of the magnetic susceptibility and transport properties of $Fe_{1+\delta}Te_{1-x}Se_x$ single crystals, Supercond. Sci. Technol. **24**, 035012 (2011).

[26] Y. Qiu, W. Bao, Y. Zhao, C. Broholm, V. Stanev, Z. Tesanovic, Y. C. Gasparovic, S. Chang, J. Hu, B. Qian, M. Fang, and Z. Mao, Spin gap and resonance at the nesting wave vector in superconducting $FeSe_{0.4}Te_{0.6}$, Phys. Rev. Lett. **103**, 067008 (2009).

[27] S. Li, C. De La Cruz, Q. Huang, Y. Chen, J. W. Lynn, J. Hu, Y.-L. Huang, F.-C. Hsu, K.-W. Yeh, M.-K. Wu, and P. Dai, First-order magnetic and structural phase transitions in $Fe_{1+y}Se_xTe_{1-x}$, Phys. Rev. B **79**, 054503 (2009).

[28] O. J. Lipscombe, G. F. Chen, C. Fang, T. G. Perring, D. L. Abernathy, A. D. Christianson, T. Egami, N. Wang, J. Hu, and P. Dai, Spin waves in the $(\pi, 0)$ magnetically ordered iron chalcogenide $Fe_{1.05}Te$, Phys. Rev. Lett. **106**, 057004 (2011).

[29] K. Terao, T. Kashiwagi, T. Shizu, R. A. Klemm, and K. Kadowaki, Superconducting and tetragonal-to-orthorhombic transitions in single crystals of $FeSe_{1-x}Te_x (0 \leq x \leq 0.61)$, Phys. Rev. B **100**, 224516 (2019).

[30] See Supplemental Materials at http://link.aps.org/supplemental/10.1103/fbfp-7gw6 for more details on sample growth, characterizations, and inelastic neutron scattering experiments, which includes Refs. [10,29,31–33].

[31] T. J. Liu, X. Ke, B. Qian, J. Hu, D. Fobes, E. K. Vehstedt, H. Pham, J. H. Yang, M. H. Fang, L. Spinu, P. Schiffer, Y. Liu, and Z. Q. Mao, Charge-carrier localization induced by excess Fe in the superconductor $Fe_{1+y}Te_{1-x}Se_x$, Phys. Rev. B **80**, 174509 (2009).

[32] Y. Sun, T. Taen, T. Yamada, S. Pyon, T. Nishizaki, Z. Shi, and T. Tamegai, Multiband effects and possible Dirac fermions in $Fe_{1+y}Te_{0.6}Se_{0.4}$, Phys. Rev. B **89**, 144512 (2014).

[33] H. Wo, B. Pan, D. Hu, Y. Feng, A. D. Christianson, and J. Zhao, Spin correlations in the parent phase of $Li_{1-x}Fe_xODFeSe$, Phys. Rev. Lett. **134**, 016501 (2025).

[34] Y. Li, Z. Yin, X. Wang, D. W. Tam, D. L. Abernathy, A. Podlesnyak, C. Zhang, M. Wang, L. Xing, C. Jin, K. Haule, G. Kotliar, T. A. Maier, and P. Dai, Orbital selective spin excitations and their impact on superconductivity of $LiFe_{1-x}Co_xAs$, Phys. Rev. Lett. **116**, 247001 (2016).

[35] T. Chen, Y. Chen, A. Kreisel, X. Lu, A. Schneidewind, Y. Qiu, J. T. Park, T. G. Perring, J. R. Stewart, H. Cao, R. Zhang, Y. Li, Y. Rong, Y. Wei, B. M. Andersen, P. J. Hirschfeld, C. Broholm, and P. Dai, Anisotropic spin fluctuations in detwinned FeSe, Nat. Mater. **18**, 709 (2019).

[36] A. Kreisel, B. M. Andersen, and P. J. Hirschfeld, Itinerant approach to magnetic neutron scattering of FeSe: Effect of orbital selectivity, Phys. Rev. B **98**, 214518 (2018).

[37] T. Shimojima, Y. Suzuki, T. Sonobe, A. Nakamura, M. Sakano, J. Omachi, K. Yoshioka, M. Kuwata-Gonokami, K. Ono, H. Kumigashira, A. E. Böhmer, F. Hardy, T. Wolf, C. Meingast, H. V. Löhneysen, H. Ikeda, and K. Ishizaka, Lifting of xz/yz orbital degeneracy at the structural transition in detwinned FeSe, Phys. Rev. B **90**, 121111(R) (2014).

[38] M. Yi, H. Pfau, Y. Zhang, Y. He, H. Wu, T. Chen, Z. R. Ye, M. Hashimoto, R. Yu, Q. Si, D.-H. Lee, P. Dai, Z.-X. Shen, D. H. Lu, and R. J. Birgeneau, Nematic energy scale and the missing electron pocket in FeSe, Phys. Rev. X **9**, 041049 (2019).

[39] K. Nakayama, R. Tsubono, G. N. Phan, F. Nabeshima, N. Shikama, T. Ishikawa, Y. Sakishita, S. Ideta, K. Tanaka, A. Maeda, T. Takahashi, and T. Sato, Orbital mixing at the onset of high-temperature superconductivity in $FeSe_{1-x}Te_x/CaF_2$, Phys. Rev. Res. **3**, L012007 (2021).

[40] D. W. Tam, Z. Yin, Y. Xie, W. Wang, M. B. Stone, D. T. Adroja, H. C. Walker, M. Yi, and P. Dai, Orbital selective spin waves in detwinned NaFeAs, Phys. Rev. B **102**, 054430 (2020).

[41] B. Pan, Y. Shen, D. Hu, Y. Feng, J. T. Park, A. D. Christianson, Q. Wang, Y. Hao, H. Wo, Z. Yin, T. A. Maier, and J. Zhao, Structure of spin excitations in heavily electron-doped $Li_{0.8}Fe_{0.2}ODFeSe$ superconductors, Nat. Commun. **8**, 123 (2017).

[42] R. Yu and Q. Si, Orbital-selective Mott phase in multiorbital models for iron pnictides and chalcogenides, Phys. Rev. B **96**, 125110 (2017).

[43] A. B. Morfoot, T. K. Kim, M. D. Watson, A. A. Haghighirad, S. J. Singh, N. Bultinck, and A. I. Coldea, Resurgence of superconductivity and the role of dxy hole band in $FeSe_{1-x}Te_x$, Commun. Phys. **6**, 362 (2023).

[44] A. Kreisel, S. Mukherjee, P. J. Hirschfeld, and B. M. Andersen, Spin excitations in a model of FeSe with orbital ordering, Phys. Rev. B **92**, 224515 (2015).

[45] C. Zhang, L. W. Harriger, Z. Yin, W. Lv, M. Wang, G. Tan, Y. Song, D. L. Abernathy, W. Tian, T. Egami, K. Haule, G. Kotliar, and P. Dai, Effect of pnictogen height on spin waves in iron pnictides, Phys. Rev. Lett. **112**, 217202 (2014).

[46] J. Huang *et al.*, Correlation-driven electronic reconstruction in $FeTe_{1-x}Se_x$, Commun. Phys. **5**, 29 (2022).

[47] Z. K. Liu, M. Yi, Y. Zhang, J. Hu, R. Yu, J.-X. Zhu, R.-H. He, Y. L. Chen, M. Hashimoto, R. G. Moore, S.-K. Mo, Z. Hussain, Q. Si, Z. Q. Mao, D. H. Lu, and Z.-X. Shen, Experimental observation of incoherent-coherent crossover and orbital-dependent band renormalization in iron chalcogenide superconductors, Phys. Rev. B **92**, 235138 (2015).

[48] M. Fujita, H. Hiraka, M. Matsuda, M. Matsuura, J. M. Tranquada, S. Wakimoto, G. Xu, and K. Yamada, Progress in neutron scattering studies of spin excitations in high-T_c cuprates, J. Phys. Soc. Jpn. **81**, 011007 (2012).

[49] V. Hinkov, P. Bourges, S. Pailhès, Y. Sidis, A. Ivanov, C. D. Frost, T. G. Perring, C. T. Lin, D. P. Chen, and B. Keimer, Spin dynamics in the pseudogap state of a high-temperature superconductor, Nat. Phys. **3**, 780 (2007).

[50] M. Yi *et al.*, Observation of universal strong orbital-dependent correlation effects in iron chalcogenides, Nat. Commun. **6**, 7777 (2015).

[51] A. Kostin, P. O. Sprau, A. Kreisel, Y. X. Chong, A. E. Böhmer, P. C. Canfield, P. J. Hirschfeld, B. M. Andersen, and J. C. S. Davis, Imaging orbital-selective quasiparticles in the Hund's metal state of FeSe, Nat. Mater. **17**, 869 (2018).